Korean J. Chem. Eng., 39(3), 586-595 (2022)
DOI: 10.1007/s11814-021-0930-1

pISSN: 0256-1115
eISSN: 1975-7220

Effects of catalyst preparation methods on the performance of La_2MMnO_6 (M=Co, Ni) double perovskites in catalytic combustion of propane

Hamidreza Roozbahani, Sarah Maghsoodi†, Behrouz Raei, Amirhossein Shahbazi Kootenaei, and Zoha Azizi

Department of Chemical Engineering, Mahshahr Branch, Islamic Azad University, Mahshahr, Iran
(*Received 2 April 2021 • Revised 2 August 2021 • Accepted 15 August 2021*)

Abstract−La_2MMnO_6 (M=Co, Ni) dual perovskite oxides were synthesized by sol-gel and gel-combustion methods and tested for the total oxidation of propane. The synthesized catalysts were characterized by TPR, XRD, ICP, SEM, TEM, H_2-TPR and O_2-TPD techniques. The preparation method had a significant effect on the physicochemical properties of samples. The XRD spectra resulting from the synthesized samples revealed the formation of single-phase perovskite structure. The largest BET specific surface area related to the La_2NiMnO_6 perovskite synthesized by the gel-combustion method was obtained as 35 m^2g^{-1} after calcination at 500 °C. Based on the findings, the catalysts synthesized by the gel-combustion method showed an increase in specific surface area, oxygen capacity, reducibility and oxygen mobility compared to those synthesized by the sol-gel method. Accordingly, these catalysts revealed a better performance. The acquired results also showed that the presence of Ni improved the catalytic activity compared to Co. The La_2NiMnO_6 perovskite synthesized by the gel-combustion method with the T_{90} equal to 415 °C was found to be the most active catalyst, while the La_2CoMnO_6 double perovskite synthesized by the sol-gel method with the T_{90} equal to 474 °C demonstrated the lowest activity.

Keywords: Catalyst, Combustion, Double Perovskite, Sol-gel, Gel-combustion

INTRODUCTION

Air pollution is one of the most important environmental problems in the last century that threatens human health. Major air pollutants include sulfur oxides, nitrogen oxides, volatile organic compounds (VOCs), and particulate matter. Volatile organic compounds are liquids or solids containing organic carbon which evaporate at a remarkable rate. Following the particulate matter, these compounds have the highest abundance and variety of emissions [1].

Volatile organic compounds may not be toxic; however, they can cause devastating long-term effects on human health and the environment. The most common VOCs are halogen compounds, alkenes, aldehydes, alcohols, ketones, aromatic compounds, and ethers. High concentrations of these compounds may cause irritation, nausea, dizziness, and headaches. Because of their carcinogenicity, the importance of their abatement has drawn particular attention [2].

VOCs can react with nitrogen oxides in the atmosphere in the presence of sunlight. This reaction leads to the formation of ozone and peroxyacetyl nitrate, which in turn can cause environmental hazards. Therefore, the effective reduction of the emission of volatile gases has turned into a major and crucial issue [3,4].

More than 50% of the emitted volatile organic compounds are caused by cars, while gasoline vehicles account for a larger share compared to diesel vehicles. According to a 2001 study by Watson et al., gasoline vehicles emit four times more VOCs than diesel vehicles. Alkanes are major products of internal combustion engines [5,6].

Propane is one of the most important volatile organic compounds, which is released mainly into the environment due to the use of LPG as an alternative fuel in automobiles. Different methods have been developed to reduce the emission of volatile organic compounds. Catalytic oxidation appears to be one of the most common methods for the abatement of volatile organic compounds, through which organic pollutants are degraded and converted into non-harmful compounds [7]. Among the investigated catalysts, a mixture of perovskite metal oxides has demonstrated promising results for the oxidation of volatile organic compounds since it provides the oxidation pathway for the conversion of VOCs to CO_2 and H_2O (g) [8,9].

Perovskites are a group of compounds with general structural formula ABO_3 or A_2BO_4, which have a cubic structure. In these compounds, the larger cation A and the smaller cation B is in 12-fold and 6-fold coordination with the oxygen anions, respectively. Each oxygen atom is surrounded by two cations in site B and four cations in site A [10,11].

Perovskites have important properties, such as the stability of different valances of transition metal ions at site B, non-stoichiometric structures at sites A and B, oxygen content in the structure with high mobility, flexibility, high thermal stability, and the ability of oxygen absorption and desorption, and resistance to sulfur, phosphorus, and halogen poisoning [12,13]. The catalytic properties of perovskites depend mainly on the nature and the oxidation state of the cation at site B [13,14]. However, the inferior specific surface area of perovskites limits their efficient use in some catalytic reactions [15,16]. Thus, some studies have been done to increase the surface area of these materials, such as changing the synthesis method and/or mounting perovskites on proper supports [17,18]. Besides, the activ-

†To whom correspondence should be addressed.
E-mail: maghsoodi_mahshahr@yahoo.com

ity of perovskites can be effectively improved by partially substitution of the appropriate elements in sites A and/or B [11,14,19-21].

Double perovskite catalysts ($A_2B'B''O_6$), a subclass of perovskite oxides ABO_3, have attracted considerable interest due to their unique structure. Double perovskites may have more structural changes than single perovskites, which may result in catalytic performance enhancement. The VOC abatement activity of double perovskites is expected to be equal to or greater than that of single perovskites [16,22]. There have been few reports regarding the use of double perovskites as combustion catalysts despite the promising results mentioned and a large number of investigated formulations. Double perovskites have been studied in processes such as catalytic combustion of methane, methane steam reforming, and partial oxidation of methane [20,23,24]. The various catalytic activity of double perovskites can be due to differences in active surface area, crystalline structure, reducibility, and oxygen species [11,14,25,26].

The performance of $LaCo_{1-x}Fe_xO_3$ catalyst was compared to related single perovskites for methane catalytic combustion. As revealed by the research, a correlation has been found between the physical and chemical properties of this oxidant with its catalytic behavior. Moreover, $A_2B'B''O_6$ catalysts have more active oxide species than ABO_3 for the combustion operation based on XPS and TPR measurements [11,21,27]. Tasca et al. [26] synthesized double perovskite catalysts of La_2MMnO_6 (M=Co, Ni, Cu) using the citrate method for total oxidation of propane. The elaborated catalysts containing cation $M^{(II)}$ were adequate for propane catalytic combustion and the La_2CoMnO_6 catalyst was the most active catalyst with T_{90}~500 °C. Double perovskite catalysts such as La_2CoMnO_6 and La_2CuMnO_6 and single perovskites, including $LaCoO_3$, $LaMnO_3$, and $LaCuO_3$ were prepared and examined to evaluate the effectiveness of various VOCs removal, including toluene, ethylene, isopropyl alcohol, and acetaldehyde [28-30]. Based on experimental results, the performance of double perovskites was superior to single perovskites.

The preparation method can influence the properties of double perovskites. Studies have indicated that the $LaSrFeMo_{0.9}Co_{0.1}O_6$ catalysts synthesized by co-precipitation and sol-gel methods provide a significant catalytic capability for methane combustion at 800 °C [22]. The synthesis method can affect the texture, surface acidity, hydrogen reducibility, oxygen absorption, surface composition, and catalytic activity. The properties of $LaMnO_3$ and $La_{0.8}Sr_{0.2}MnO_3$ perovskites synthesized by sol-gel, chemical combustion, solvothermal, and spray pyrolysis methods have been studied to evaluate their catalytic activity for dilute methane combustion. The results suggest that the synthesis method can affect the physical and chemical properties of perovskites [31].

This paper examined the performance of double perovskite catalysts of La_2MMnO_6 (M=Co, Ni) synthesized by sol-gel and gel-combustion methods. Physical and chemical properties of the prepared samples were examined.

EXPERIMENTAL

1. Catalyst Preparation

The $A_2BB'O_6$ double perovskites are the catalysts used in this study with lanthanum (La) located at site A, manganese (Mn) at site B, and transition metals of nickel (Ni) or cobalt (Co) at site B′. The double perovskites were synthesized by sol-gel (SG) and gel-combustion (GC) methods. All the chemicals were purchased from Merck Company and used as received.

1-1. Sol-gel Method

A solution of distilled water, citric acid, and ethylene glycol was prepared. Then, manganese nitrate ($Mn(NO_3)_2{\cdot}4H_2O$) and cobalt nitrate ($Co(NO_3)_2{\cdot}6H_2O$) or nickel nitrate ($Ni(NO_3)_2{\cdot}6H_2O$) were added to the solution and stirred to obtain a clear and homogeneous solution. In the next step, lanthanum nitrate ($La(NO_3)_3{\cdot}6H_2O$), was added to the solution followed by heating at 70 °C and stirring to convert the mixture into a gel. For samples, the molar ratio of citric acid to ethylene glycol was chosen to be 1, while the molar ratio of La, Mn and M (M=Co or Ni) was taken 2 : 1 : 1. The gelation process was continued until the materials were completely dried. Then, the product was powdered. The calcination process was conducted at static air at 500 °C for 4 hours. The sample was crushed and meshed to obtain a proper size of the catalyst.

1-2. Gel-combustion Method

Sorbitol as the fuel and lanthanum nitrate, manganese nitrate, and cobalt nitrate or nickel nitrates were utilized in the gel-combustion method to synthesize La_2MMnO_6 (M=Co, Ni) double perovskite catalysts. A mixture of all the precursors was heated at 75 °C under stirring to obtain a completely homogeneous and gel-like mixture. In the initial gel, the molar ratios of La, Mn and M (M=Co or Ni) were 2 : 1 : 1, while the molar ratio of sorbitol to La was 5. The product was then cooled at room temperature for 15 minutes. Afterward, the resulting gel was transferred to a microwave oven for the combustion operation. Following the combustion, the synthesized product was placed in a static air furnace for 4 h at 500 °C.

2. Catalysts Characterization

Different physical and chemical properties of the samples were characterized using various methods such as X-Ray diffraction (XRD), Fourier transform-infrared spectroscopy (FTIR), scanning electron microscopy (SEM), transmission electron microscopy (TEM), temperature-programmed reduction (TPR), and BET specific surface area (S_{BET}) measurement. The crystalline structure of catalysts was examined with X-ray diffraction (XRD) analysis by a diffractometer (Philips Co., Model: PW1800) using Cu Kα radiation (λ=0.1541 nm). The diffraction intensity was recorded for all samples in the range of $10^o<2\theta<80^o$ with a step size equal to 0.03° and a time of 2 seconds per step. The resulting spectra were identified by comparing the data from the Joint Committee on Powder Diffraction Standards (JCPDS) followed by applying the X'Pert HighScore software to interpret the spectra. The mean particle size (d_{XRD}) was obtained by the Scherrer equation. The Debye-Scherrer equation was used to calculate the average size of crystals based on the data of the X-ray diffraction patterns.

$$d_{XRD}=\frac{k\lambda}{\beta\cos(\theta)} \quad (1)$$

where β is the index peak width at half the peak height; λ is the x-ray wavelength (0.15418 nm); θ is the angle between the diffracted and incoming beams; and d_{XRD} is the size of the crystals in nanometers. The specific surface area of the synthesized catalysts was

determined using the BET analysis by an apparatus of Nova Station A model made by Quantachrome NovaWin2 Company. For analysis, the sample was heated before testing from ambient temperature to 300 °C in nitrogen flow with a flow rate of 20 cm^3/min and kept at this temperature for 2 h. Then, the adsorption of nitrogen gas was conducted at liquid nitrogen temperature (–196 °C). The FTIR spectra were acquired by the Perkin Elmer Spectrum apparatus using the KBr-tablet technique. The size of particles and the morphology of the prepared catalysts were determined by scanning electron microscopy (SEM) technique (TESCAN Vega Model) and transmission electron microscopy (TEM) analysis (Zeiss-EM10C-100 KV model). The chemical composition of the samples was analyzed through inductively coupled plasma analysis (ICP) by a Perkin-Elmer spectrometer.

TPR analysis was performed by BELCAT A device. 25 mg of the synthesized sample was heated under a stream of dry air with a flow rate of 20 cm^3/min from the ambient temperature to 600 °C and kept at this temperature for 1 h. The temperature of the sample was then lowered to the ambient temperature under the same gas flow. After degassing, the sample was reduced under a flow of 7% H_2 in Ar. The gas mixture flow rate was adjusted at 10 cm^3/min and the temperature was raised by a 10 °C/min rate up to 900 °C. Finally, the amount of hydrogen consumed in the reduction process was calculated by integrating the areas under the TPR curves.

O_2 temperature-programmed desorption (O_2-TPD) was done by a Micrometer 2920 device equipped with a quadruple mass spectrometer. For this purpose, 50 mg sample was first pretreated with a flow of 20% O_2 in He at 600 °C for 1 h and then cooled to 40 °C. The sample was kept at 40 °C in 20% O_2/He for 1 h and then desorption of physisorbed O_2 was done by a flow of He for 1 h. Finally, O_2-TPD was performed by heating the sample to 600 °C with a ramping rate of 10 °C/min under a flow of He.

3. Catalytic Tests

The catalyst activity test was performed in a fixed bed quartz microreactor with a length of 80 cm, an inner diameter of 7 mm, and an outer diameter of 9 mm. The feed gas contained 4,000 ppm propane in dry air. The catalyst used in each experiment (100 mg) was mounted at the center of the reactor on acid-washed quartz wool. The catalyst was heated under a flow of dry air with a flow rate of 50 cm^3/s and a heating rate of 10 °C/min from room temperature to 500 °C. The reactor was then subjected to specific temperature points under the feed gas flow of 50 cm^3/s. After stable conditions were established at each temperature, the amount of effluent gases from the reactor was analyzed online by a gas chromatograph (Varian CP-3800). The conversion of propane at each temperature was determined using the difference in propane concentration at the input and output relative to the input concentration, which were drawn and analyzed in the form of catalyst activity diagrams.

RESULTS AND DISCUSSION

1. Catalyst Characterization

1-1. XRD, Chemical Composition and Specific Surface Area

The XRD patterns of La_2CoMnO_6 and La_2NiMnO_6 double perovskites synthesized by sol-gel (SG) and gel-combustion (GC) methods after calcination at 500 °C were obtained as shown in Fig. 1. For a comparison, the XRD pattern of $LaMnO_3$ is also given in Fig. 1. All the double perovskites showed reflexions ascribed to the hexagonal $LaMnO_3$ perovskite standard patterns (JCPDS card 54-1275). The diffraction peaks of La_2CoMnO_6 and La_2NiMnO_6 samples are mainly located at 23°, 33°, 40°, 47°, 58°, 68°, and 78°, which are similar to $LaMnO_3$. No diffraction peaks related to Ni and Co elements were detected in all samples, indicating the formation of double perovskites with single phase. These patterns are consistent with the results obtained by a previous work on $A_2BB'O_6$ double perovskites [21,25].

The relative crystallinity of the samples was measured on the base of La_2NiMNO_6-SG and the obtained results showed the relative crystallinity was in the order of La_2NiMnO_6-GC (100%)> La_2NiMnO_6-SG (87%)>La_2CoMnO_6-GC (72%)>La_2CoMnO_6-SG (66%). The higher the crystallinity, the larger the size of crystals [32]. Therefore, based on the crystallinity results, one can claim that a specific sample synthesized by the combustion method has higher

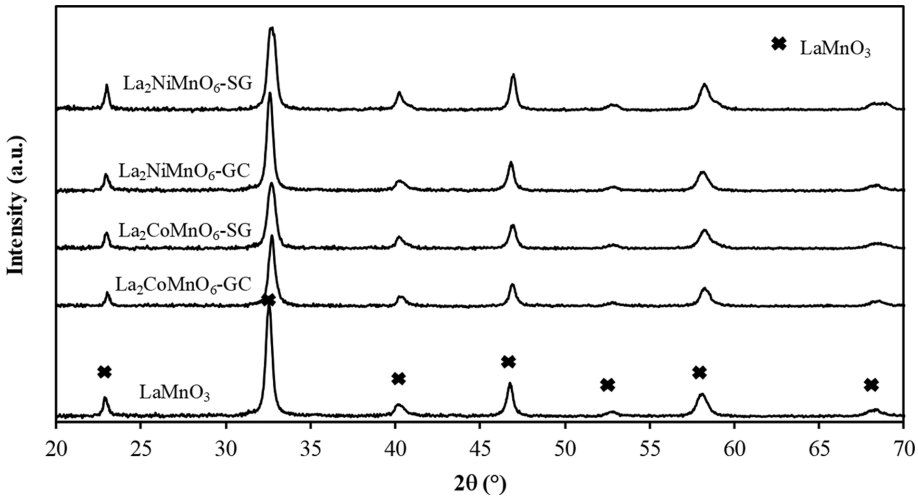

Fig. 1. XRD patterns of La_2MMnO_6 (M=Co, Ni) double perovskites calcined at 500 °C.

Table 1. XRD, BET and ICP results of La_2MMnO_6 perovskites (M=Co, Ni)

Catalyst sample	Max. height	Crystal size (nm)	Specific surface area ($m^2\ g^{-1}$)	Real value (at.%)			Nominal value (at.%)		
				La	Mn	M[a]	La	Mn	M[a]
La_2CoMnO_6-GC	2,078	17.3	28.7	51.7	22.2	26.1	50	25	25
La_2CoMnO_6-SG	1,942	15.2	22.9	52.3	21.8	25.9	50	25	25
La_2NiMnO_6-GC	2,940	20.5	35.4	52.9	21.7	25.4	50	25	25
La_2NiMnO_6-SG	2,549	18.7	22.3	53.4	22.3	24.3	50	25	25

[a]M=Co or Ni

crystallinity as compared to corresponding sample synthesized by the sol-gel method. For instance, La_2NiMnO_6 synthesized by the combustion method has higher crystallinity than that of La_2NiMnO_6 synthesized by the sol-gel method.

The mean size of the La_2MMnO_6 (M=Co, Ni) crystals synthesized by the sol-gel and gel-combustion methods was calculated by the Debye-Scherrer equation (Eq. (1)) and the acquired results are shown in Table 1. The average size of the synthesized crystals falls into the range of 15-20 nm. This observation demonstrates that the combustion method results in the formation of larger particles, in agreement with the crystallinity results.

The chemical composition of the synthesized samples was measured by ICP and the acquired results are given in Table 1. The results show that the measured values of the elements are close to nominal ones. Some little differences between experimental and theoretical values are due to formation of some unsaturated cations during the synthesis process which influence on the ICP results. The composition values are in agreement with those reported in literature [14,33].

The BET specific surface area (S_{BET}) of the elaborated catalysts are displayed in Table 1. Perovskites usually have small specific surface areas. However, the increased specific surface area is recognized as a factor that improves the performance of perovskites and increases their level of activity [32].

Based on the data shown in Table 1, a specified perovskite synthesized by the gel-combustion method has greater crystal size and specific surface area than that of the corresponding sample synthesized by sol-gel method. La_2NiMnO_6-GC double perovskite has the largest specific surface area, which in turn increases its catalytic activity compared to other double perovskites.

In general, the gel-combustion method increases the mean specific surface area of perovskites due to the evolution of a large amount of gas during the combustion reaction. The mean surface area of the particles obtained is not so large; however, the decomposition of the precursors and the fuel during the combustion reaction leads to the release of large amounts of gaseous products in a short period of time, causing the formation of many voids and pores, which accordingly increases porosity and surface area [34,35].

1-2. FTIR Characterization

FTIR test was conducted on the synthesized samples to confirm the formation of perovskite structure. As illustrated in Fig. 2, the vibrational bands of the samples between 400 cm^{-1} and 600 cm^{-1} can be attributed to the stretching and flexural vibrations of the B-O band in the BO_6 octahedral similar to the other $A_2BB'O_6$ structures according to previous studies [36,37]. The octagonal

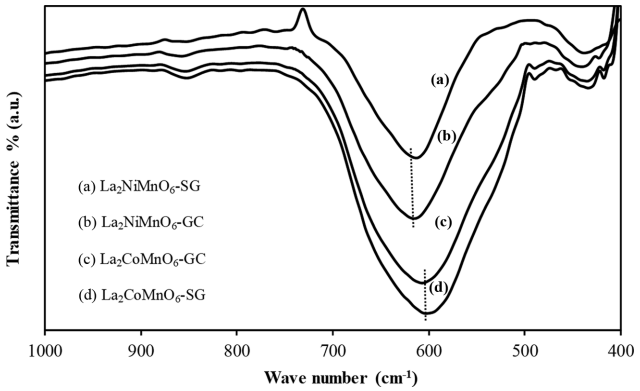

Fig. 2. FTIR spectra of synthesized La_2MMnO_6 (M=Co, Ni) double perovskites.

moieties of the BO_6 are usually stronger bands in these structures, which are associated with two stretching and anti-symmetric characteristics of the modes [36]. The vibrational behavior in double perovskites is highly complex due to the presence of two metal cations B and B′ with different charges and sizes at the octagonal locations of the unit cell. However, the Mn^{4+}-O band is considered to be somewhat stronger than the other bands despite the important vibrational bonds between the BO_6 octagons (i.e., Co-O or Ni-O bands) [38]. Hence, the strong and wide band located at the (V3) ~ 600 cm^{-1} can be more attributed to the anti-symmetric stretching of the polyhedron MnO_6. Actually, Ni-O and Co-O bands with weaker intensities are overlapped with Mn-O band.

Based on the data obtained from Table 2, the change in stretching motion of V3 towards higher energy level from Ni to Co can be related to the strengthening of Mn^{4+}-O bonds. The order of ionic radii is as follows: r(Mn)>r(Co)>r(Ni) [21]. Substituting Mn by Ni or Co with lower ionic radii compared to Mn results in the stretching of Mn-O bonds in the lattice and accordingly increases the internal pressure on the perovskite lattice [37,39]. On the other hand, the substitution of Mn by Ni with lower ionic radii com-

Table 2. FTIR spectroscopic data of La_2MMnO_6 (M=Co, Ni) prepared by sol-gel method

Oxides	Infrared frequencies and intensities (cm^{-1})	
	V_3	V_4
La_2NiMnO_6	613	438
La_2CoMnO_6	603	434

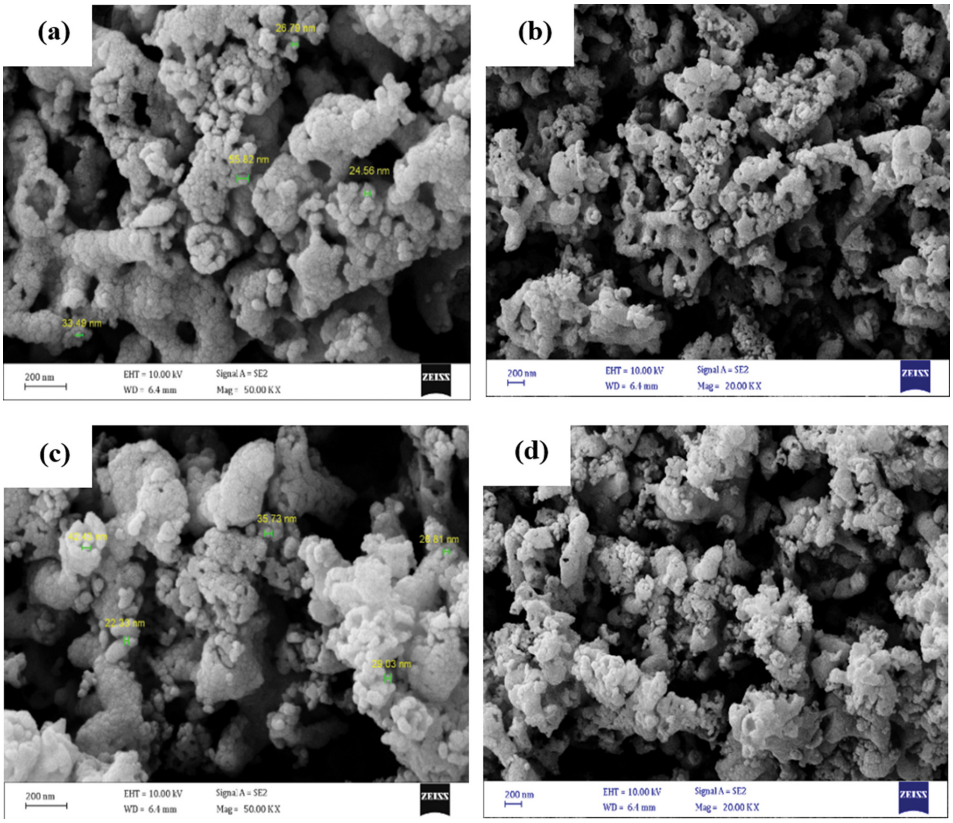

Fig. 3. SEM micrographs of the samples: (a) La_2NiMnO_6-GC, (b) La_2NiMnO_6-SG, (c) La_2CoMnO_6-GC, and (d) La_2CoMnO_6-SG.

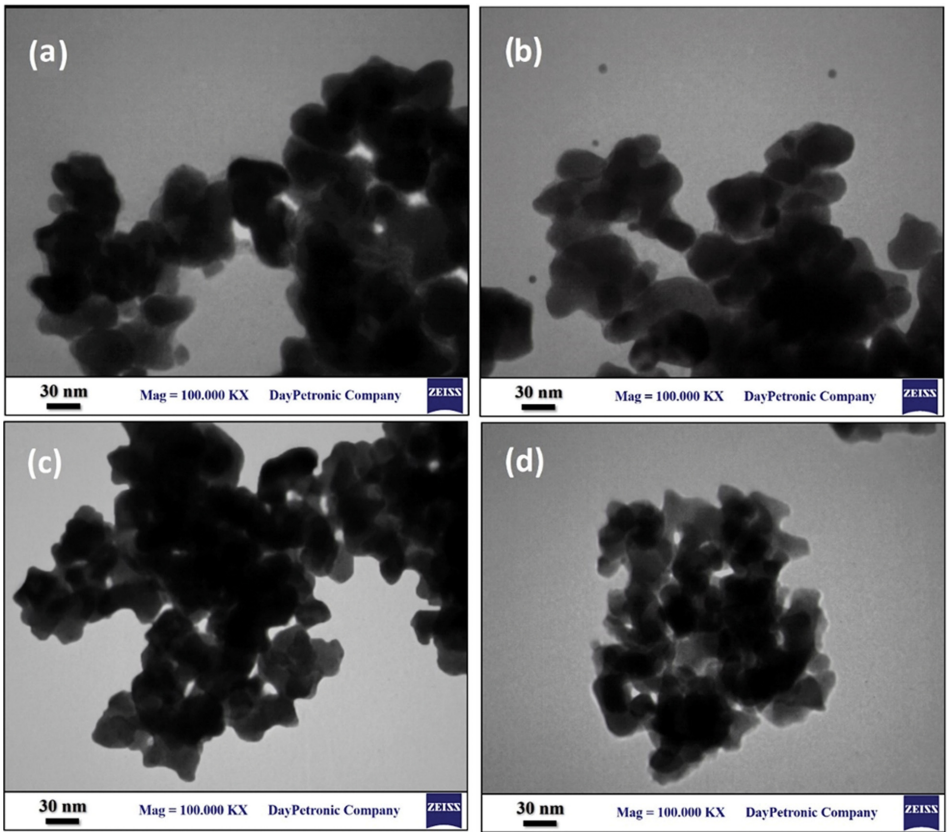

Fig. 4. TEM images of the samples: (a) La_2NiMnO_6-GC, (b) La_2NiMnO_6-SG, (c) La_2CoMnO_6-GC, and (d) La_2CoMnO_6-SG.

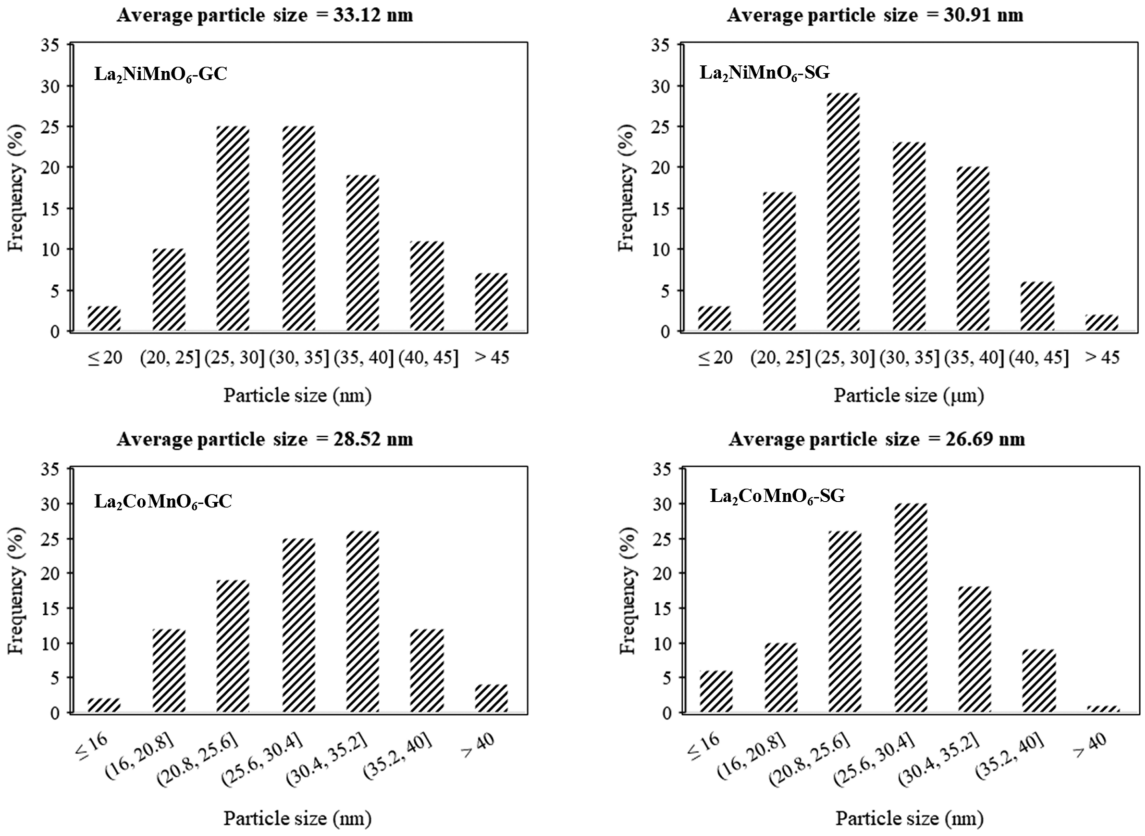

Fig. 5. Particle size distribution of La_2MMnO_6 (M=Co, Ni) samples prepared by SG and GC methods.

pared to Co results in the more stretch of Mn-O bonds, which is accompanied by an increase in the Mn-O absorption wave number. The strengthening of Mn-O bonds results in the increase of crystal size as demonstrated by Debye-Scherrer equation results (Table 1).

1-3. Morphology Investigation

The SEM images were acquired to study the morphology of double perovskites synthesized by the sol-gel and gel-combustion methods as presented in Fig. 3. All samples possess a spongy, dense, and porous structure. As can be seen in the figures, there are some pores and cavities in the structure of the perovskites due to the production of large amounts of gas during the synthesis process [34,40]. The size of the synthesized particles is displayed on the images that the average particle size is approximately in the range of 22 to 56 nm.

The TEM images of the samples are illustrated in Fig. 4 to further investigate the morphology of the double perovskites with higher magnification. The images of the obtained materials suggest the presence of non-spherical nanoparticles. One can realize that larger particles are actually formed of much smaller particles. The quantitative investigation of TEM images was done in order to obtain the particle size distribution of the synthesized samples, and the acquired results are given in Fig. 5. According to the obtained results, the average crystal size of the particles seems to correspond well to the crystal size estimated by XRD so that the double perovskites synthesized by the gel-combustion method have larger particle size.

1-4. Temperature-Programmed Reduction by Hydrogen (H_2-TPR)

H_2-TPR can provide some information such as the oxidation of metal ions, activity of the surface ions and lattice oxygen, and cata-

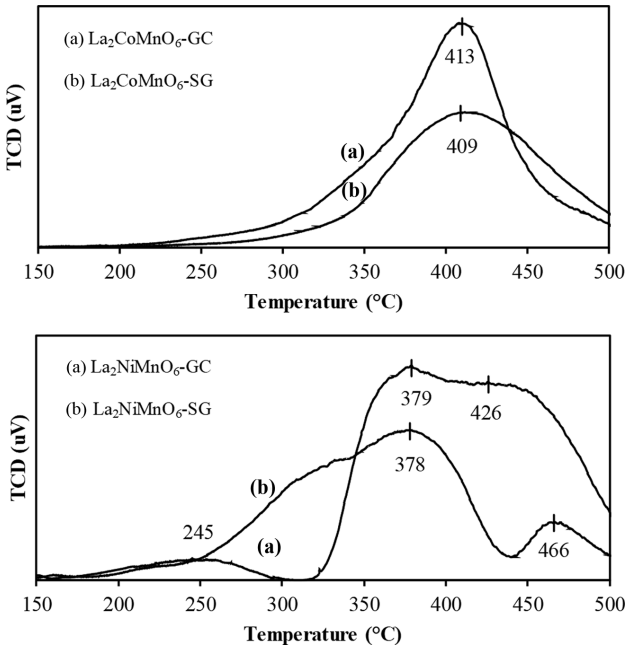

Fig. 6. H_2-TPR profiles of La_2MMnO_6 (M=Co, Ni) catalysts prepared by GC and SG methods.

lyst stability. The TPR profiles of the elaborated samples are plotted in Fig. 6. The high-valence metal ions are reduced by H_2 to low-valence ions or metal atoms during the H_2-TPR process. The oxygen ions at the surface and inside of the lattice are also reduced. Thus, the reduction peaks reflect the activity of oxygen species in addition to the oxidation feature of metal ions [41]. In general, the area under the curve represents the amount of hydrogen consumed during the reaction. The amount of hydrogen consumed in the reduction process is calculated by integrating the area under the TPR curve. Higher catalyst oxidation is associated with larger area of the reduction peak as well as lower peak temperature. The perovskite reduction process can be an important factor in determining catalyst activity [14,15,21].

La is not reduced generally in H_2-TPR process. Thus, reduction peaks of the La-based perovskites are mainly associated with the reduction of B-site metals [40]. The obtained results in Fig. 5 suggest that the reduction peak of La_2CoMnO_6 is located between 300 °C and 500 °C, which is due to the reduction of $Co^{3+}\rightarrow Co^{2+}\rightarrow Co^0$ as well as $Mn^{4+}\rightarrow Mn^{3+}$. The complete reduction of manganese cations and the formation of metallic manganese is not possible thermodynamically [42].

The reduction peaks occur between 200 °C and 500 °C in the case of La_2NiMnO_6, which is due to the reduction of $Ni^{3+}\rightarrow Ni^{2+}\rightarrow Ni^0$ and $Mn^{4+}\rightarrow Mn^{3+}$. The reduction peak at low temperature is caused by the reduction of excess oxygen and chemisorbed oxygen on the surface of the catalyst [42,43].

Double perovskites synthesized by the gel-combustion method consume more hydrogen, and naturally, possess higher reducibility. These perovskites have a higher peak and a larger area under the curve. Moreover, their peak temperature is lower than that of the double perovskites synthesized by the sol-gel method. La_2NiMnO_6-GC has the lowest reduction temperature among the investigated samples.

Table 3 shows the total amount of H_2 consumed in H_2-TPR. The increase of H_2 consumption in H_2-TPR shows the increase of oxygen storage capacity. Based on the obtained data, the samples synthesized by the gel-combustion method can provide more active oxygen. Based on these measurements, the reducibility and oxygen capacity of double perovskites are as the following order: La_2NiMnO_6-GC>La_2CoMnO_6-GC>La_2NiMnO_6-SG>La_2CoMnO_6-SG.

1-5. O_2 Temperature-programmed Desorption (O_2-TPD)

The behavior of the surface oxygen species was explored by O_2-TPD technique, and the acquired results are shown in Fig. 7. All samples show a broad peak in the range of 200 to 500 °C, resulting from the desorption of chemisorbed species O^{2-}/O^- created by O_2, which is adsorbed on catalyst surface vacancies [14,21,25]. The

Table 3. Results of H_2-TPR of catalysts obtained by GC and SG methods

Catalyst	mmol/$g_{catalyst}$
La_2NiMnO_6-GC	2.00
La_2CoMnO_6-GC	1.62
La_2NiMnO_6- SG	1.32
La_2CoMnO_6- SG	1.28

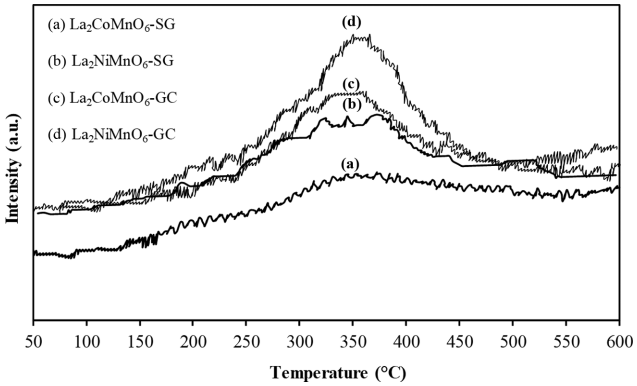

Fig. 7. O_2-TPD profiles of the synthesized La_2MMnO_6 (M=Co, Ni) catalysts prepared by GC and SG methods.

samples synthesized by the gel-combustion method, especially the La_2NiMnO_6-GC sample, have larger peaks, indicating that this method generates a great deal of oxygen vacancies, which promotes the desorption and mobility of oxygen. Based on the O_2-TPD results, the oxygen mobility of double perovskites is in the order of La_2NiMnO_6-GC>La_2CoMnO_6-GC>La_2NiMnO_6-SG>La_2CoMnO_6-SG, in agreement with H_2-TPR where the same order was observed for the oxygen capacity of samples.

2. Catalytic Propane Combustion

The conversion of propane at each temperature was calculated using the difference between the concentration of propane at the input and the output relative to the input concentration (Eq. (2)) in order to evaluate the activity of double perovskite catalysts.

$$\text{Conversion (\%)} = \frac{[\text{Propane}]_{in} - [\text{Propane}]_{out}}{[\text{Propane}]_{in}} \times 100 \quad (2)$$

According to Fig. 8(a), the conversion for propane was measured and plotted as a function of temperature. As can be seen, the double perovskite oxides have potential catalytic benefits for propane combustion. All catalysts with an S-shaped curve show a relatively steep slope for the conversion of propane as a function of the reaction temperature. According to the obtained diagrams, the catalytic performance of double perovskites is directly related to the temperature, so that the propane conversion increases as the temperature rises. Besides, double perovskites provide better catalytic performance at higher temperature, while the conversion decreases significantly at low temperature. As can be seen in the diagram, the propane conversion rate is less than 10% at temperature below 275 °C.

In oxidation reactions, CO_2 is produced with small amounts of CO. As shown in Fig. 8(b), as typical results, the amount of converted propane (ppm) is nearly one-third of he amount of produced CO_2 (ppm), for La_2NiMnO_6-GC catalyst. In all the catalytic tests, carbon balances were close to 100% (98.5%-100%). This clearly shows that, within the high detection limits of the GC, propane is not converted to other detectable hydrocarbons.

Table 4 shows the quantitative comparison of the activity of the synthesized catalysts and the activation energies at T_{10}, T_{50}, and T_{90} as the temperature required to convert 10%, 50%, and 90% of propane with a concentration of 4,000 ppm. The temperatures of T_{10},

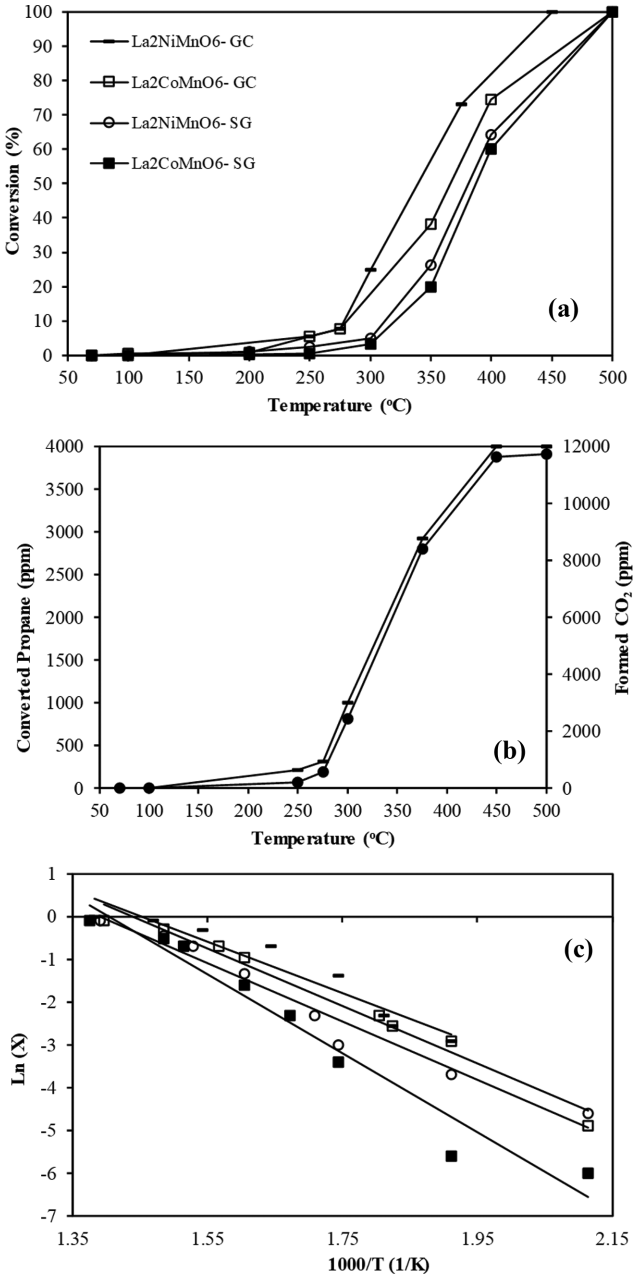

Fig. 8. (a) Catalytic activity of catalysts in the combustion of propane, (b) amount of converted propane (ppm) and formed CO_2 (ppm) as a function of reaction temperature over La_2NiMnO_6-GC catalyst, and (c) Arrhenius plots of reaction rates over La_2MMnO_6 (M=Co, Ni).

T_{50}, and T_{90} for the La_2NiMnO_6-GC catalyst are 279 °C, 335 °C, and 407 °C, respectively. This catalyst has a better performance compared to other catalysts, so its temperature for a specific conversion is lower than other catalysts. The activity rates of double catalysts in the propane conversion are, respectively, as follows:

La_2NiMnO_6-GC>La_2CoMnO_6-GC>La_2NiMnO_6-SG>La_2CoMnO_6-SG

The reaction kinetics were studied assuming steady state and the first-order reaction was used to examine the kinetic parameters. The activation energy of the perovskites synthesized was calculated for the C_3H_8 combustion reaction. The function of Ln(X) vs. (1,000/T) at different temperature (T) and C_3H_8 conversion (X) is plotted in Fig. 8(c) to determine the apparent activation energy. The values of apparent activation energy (E_a) were then calculated using the Arrhenius equation based on the straight line slope (Table 4). The double perovskites synthesized by the gel-combustion method have the lowest activation energy compared to those synthesized by the sol-gel method. The catalysts with lower activation energy need lower temperature for oxidation. The lowest E_a value was obtained for La_2NiMnO_6-GC as 49.9 kJ/mol and the highest E_a value was achieved for the La_2CoMnO_6-SG. The lower La_2NiMnO_6-GC activation energy compared to other double catalysts indicates the significant performance of this catalyst in oxidation of propane.

Based on previous research, double perovskite catalysts provide higher concentration of lattice oxygen, and thus, they show further activity. Double perovskites have higher lattice oxygen due to their special surface properties, which leads to their higher activity rate. Besides, reactive oxygen species on the catalyst surface play a crucial role in the oxidation of propane since they directly engage in the oxidation mechanism [40]. The synthesis method and calcination also affect the activity of catalysts. On the other hand, the nature of site B cations and the oxidation state also influence the catalytic activity of $La_2M^{II}Mn^{IV}O_6$ oxides [32].

According to analyses results, the synthesized samples showed different crystallinity, BET surface area, reducibility, oxygen capacity and oxygen mobility, which can influence the catalytic activity. La_2CoMnO_6-SG and La_2CoMnO_6-GC samples possessing the highest BET surface areas showed the best performance in the catalytic combustion of propane. Nonetheless, there was no direct correlation between activity and crystallinity, indicating crystallinity is less important compared to surface area, reducibility, oxygen capacity and oxygen mobility. On the other hand, the H_2-TPR and O_2-TPD results showed that oxygen mobility, oxygen capacity and reducibility of the samples were in the order of La_2NiMnO_6-GC>

Table 4. Temperatures at 10% (T_{10}), 50% (T_{50}) and 90% (T_{90}) conversion of propane and activation energies over the La_2MMnO_6 (M=Co, Ni) perovskites synthesized by the sol-gel method and gel-combustion

Sample	Catalytic activity in terms of conversion temperature (°C)			Activation energy (kJ/mol)
	T_{10} (°C)	T_{50} (°C)	T_{90} (°C)	
La_2NiMnO_6-GC	279	335	407	49.9
La_2NiMnO_6-SG	312	381	446	56.5
La_2CoMnO_6-GC	281	365	443	55.7
La_2CoMnO_6-SG	325	387	454	76.6

La_2CoMnO_6-GC>La_2NiMnO_6-SG>La_2CoMnO_6-SG, which were the same order with the catalytic activity. The active oxygen (O^{2-} species) in the structure of perovskite comes from the reduction of bulk cations [21,23,25]. As demonstrated in the H_2-TPR results, the reducibility and oxygen capacity of the perovskites followed a sequence of La_2NiMnO_6-GC>La_2CoMnO_6-GC>La_2NiMnO_6-SG> La_2CoMnO_6-SG, in agreement with the catalytic activity results. On the other hand, the higher oxygen mobility facilitates O^{2-} species accessibility to propane and accordingly results in activity improvement. Thus, the increased oxygen mobility accelerates the movement of oxygen species from interior to surface and makes them more available to propane.

CONCLUSION

The performance of all catalysts was 100% above 500 °C based on the research results and the entire propane was converted to CO_2 and H_2O. In addition, as demonstrated, double perovskite catalysts synthesized by gel-combustion method performed better, indicating the superiority of this method in comparison to the sol-gel method. La_2NiMnO_6 synthesized by the gel-combustion method demonstrated the best performance, showing higher activity for propane combustion. This can be attributed to the larger specific surface area of this perovskite than other synthesized perovskites. However, the larger specific surface area alone cannot explain the better performance of perovskites. Rather, other factors, such as better reducibility, better oxygen mobility and increased oxygen storage capacity, affected the catalytic activity of La_2NiMnO_6 synthesized by the gel-combustion method. According to the results obtained regarding the activity of catalysts and based on separately comparing each method, one can realize that nickel performs better than cobalt due to higher surface area, higher amounts of oxygen species, better reducibility and oxygen mobility.

REFERENCES

1. L. K. Wang, N. C. Pereira and Y.-T. Hung, *Air pollution control engineering*, Springer (2004).
2. Y. Huang, S. S. H. Ho, Y. Lu, R. Niu, L. Xu, J. Cao and S. Lee, *Molecules*, **21**, 56 (2016).
3. S. L. Suib, *New and future developments in catalysis: Catalysis for remediation and environmental concerns*, Newnes (2013).
4. M. S. Kamal, S. A. Razzak and M. M. Hossain, *Atmos. Environ.*, **140**, 117 (2016).
5. W. B. Li, W. B. Chu, M. Zhuang and J. Hua, *Catal. Today*, **93-95**, 205 (2004).
6. W. B. Li, J. X. Wang and H. Gong, *Catal. Today*, **148**, 81 (2009).
7. S. Ojala, N. Koivikko, T. Laitinen, A. Mouammine, P. K. Seelam, S. Laassiri, K. Ainassaari, R. Brahmi and R. L. Keiski, *Catalysts*, **5**, 1092 (2015).
8. G. Sinquin, C. Petit, J. P. Hindermann and A. Kiennemann, *Catal. Today*, **70**, 183 (2001).
9. W. P. Stege, L. E. Cadús and B. P. Barbero, *Catal. Today*, **172**, 53 (2011).
10. P. Esmaeilnejad-Ahranjani, A. Khodadadi, H. Ziaei-Azad and Y. Mortazavi, *Chem. Eng. J.*, **169**, 282 (2011).
11. D. Liang, H. Huang, J.-L. Liu and H.-L. Wang, *Inorg. Chem. Commun.*, **127**, 108533 (2021).
12. R. Spinicci, A. Delmastro, S. Ronchetti and A. Tofanari, *Mater. Chem. Phys.*, **78**, 393 (2003).
13. J. Zheng, X. Lang and C. Wang, *ACES*, **4**, 367 (2014).
14. Y. Wu, B. Chu, M. Zhang, Y. Yi, L. Dong, M. Fan, G. Jin, L. Zhang and B. Li, *Appl. Surf. Sci.*, **481**, 1277 (2019).
15. D. Ferri and L. Forni, *Appl. Catal. B: Environ.*, **16**, 119 (1998).
16. X. Tan, N. Han, H. Chen, L. Su, C. Zhang and Y. Li, *Ceram. Int.*, **47**, 8762 (2021).
17. N. K. Labhsetwar, A. Watanabe, R. B. Biniwale, R. Kumar and T. Mitsuhashi, *Appl. Catal. B: Environ.*, **33**, 165 (2001).
18. D. L. Chen, K. L. Pan and M. B. Chang, *J. Environ. Sci.*, **56**, 131 (2017).
19. S. Yoon, A. E. Maegli, L. Karvonen, S. K. Matam, A. Shkabko, S. Riegg, T. Großmann, S. G. Ebbinghaus, S. Pokrant and A. Weidenkaff, *J. Solid State Chem.*, **206**, 226 (2013).
20. M. de Santana Santos, R. Frety, L. Lisi, S. Cimino and S. Teixeira *Brandão, Fuel*, **292**, 120187 (2021).
21. Y. Wu, H. Liu, G. Li, L. Jin, X. Li, X. Ou, L. Dong, G. Jin and B. Li, *Appl. Surf. Sci.*, **508**, 145158 (2020).
22. P. K. Gallagher, D. W. Johnson, E. M. Vogel and F. Schrey, *Mater. Res. Bull.*, **10**, 623 (1975).
23. P. V. Tuza and M. M. V. M. Souza, *Catal. Lett.*, **146**, 47 (2016).
24. I. Popescu, Y. Wu, P. Granger and I.-C. Marcu, *Appl. Catal. A: Gen.*, **485**, 20 (2014).
25. J. A. Onrubia-Calvo, B. Pereda-Ayo, U. De-La-Torre and J. R. González-Velasco, *Appl. Catal. B: Environ.*, **213**, 198 (2017).
26. J. E. Tasca, A. E. Lavat and M. G. González, *J. Asian Ceram. Soc.*, **5**, 235 (2017).
27. K. L. Pan, G. T. Pan, S. Chong and M. B. Chang, *J. Environ. Sci.*, **69**, 205 (2018).
28. Y. Wei, L. Ni, M. Li and J. Zhao, *Catal. Commun.*, **155**, 106314 (2021).
29. S. Gabra, E. J. Marek, S. Poulston, G. Williams and J. S. Dennis, *Appl. Catal. B: Environ.*, **286**, 119821 (2021).
30. X. Chen, S. A. C. Carabineiro, P. B. Tavares, J. J. M. Órfão, M. F. R. Pereira and J. L. Figueiredo, *J. Environ. Chem. Eng.*, **2**, 344 (2014).
31. C. Li, B. Liu, Y. He, C. Lv, H. He and Y. Xu, *J. Alloys Compd.*, **590**, 541 (2014).
32. N. Miniajluk, J. Trawczyński, M. Zawadzki and W. Tylus, *AMPC*, **8**, 193 (2018).
33. Y. Wu, G. Li, B. Chu, L. Dong, Z. Tong, H. He, L. Zhang, M. Fan, B. Li and L. Dong, *Ind. Eng. Chem. Res.*, **57**, 15670 (2018).
34. S. Maghsoodi, J. Towfighi, A. Khodadadi and Y. Mortazavi, *Chem. Eng. J.*, **215-216**, 827 (2013).
35. H. Liang, Y. Hong, C. Zhu, S. Li, Y. Chen, Z. Liu and D. Ye, *Catal. Today*, **201**, 98 (2013).
36. C. Q. Zhu, H. Liang, S. H. Li, Y. X. Hong and D. Ye, *Chin. J. Inorg. Chem.*, **27**, 1093 (2011).
37. N. Parvizi, N. Rahemi, S. Allahyari and M. Tasbihi, *J. Ind. Eng. Chem.*, **84**, 167 (2020).
38. F. Touahra, A. Rabahi, R. Chebout, A. Boudjemaa, D. Lerari, M. Sehailia, D. Halliche and K. Bachari, *Int. J. Hydrogen Energy*, **41**, 2477 (2016).
39. G. Pecchi, C. Campos, O. Peña and L. E. Cadus, *J. Mol. Catal. A:*

Chem., **282**, 158 (2008).
40. A. E. Lavat and E. J. Baran, *J. Alloys Compd.*, **460**, 152 (2008).
41. S. M. Lima, J. M. Assaf, M. A. Peña and J. L. G. Fierro, *Appl. Catal. A: Gen.*, **311**, 94 (2006).
42. A. E. Lavat and E. J. Baran, *Vib. Spectrosc.*, **32**, 167 (2003).
43. B. Kucharczyk, K. Adamska, W. Tylus, W. Miśta, B. Szczygieł and J. Winiarski, *Catal. Lett.*, **149**, 1919 (2019).